Carbon Dioxide Capture for Storage in Deep Geologic Formations – Results from the CO_2 Capture Project

Geologic Storage of Carbon Dioxide with Monitoring and Verification

Volume 2

Elsevier Internet Homepage – http://www.elsevier.com
Consult the Elsevier homepage for full catalogue information on all books, major reference works, journals, electronic products and services.

Elsevier Titles of Related Interest

AN END TO GLOBAL WARMING
L.O. Williams
ISBN: 0-08-044045-2, 2002

FUNDAMENTALS AND TECHNOLOGY OF COMBUSTION
F. El-Mahallawy, S. El-Din Habik
ISBN: 0-08-044106-8, 2002

GREENHOUSE GAS CONTROL TECHNOLOGIES: 6TH INTERNATIONAL CONFERENCE
John Gale, Yoichi Kaya
ISBN: 0-08-044276-5, 2003

MITIGATING CLIMATE CHANGE: FLEXIBILITY MECHANISMS
T. Jackson
ISBN: 0-08-044092-4, 2001

Related Journals:
Elsevier publishes a wide-ranging portfolio of high quality research journals, encompassing the energy policy, environmental, and renewable energy fields. A sample journal issue is available online by visiting the Elsevier web site (details at the top of this page). Leading titles include:

Energy Policy
Renewable Energy
Energy Conversion and Management
Biomass & Bioenergy
Environmental Science & Policy
Global and Planetary Change
Atmospheric Environment
Chemosphere – Global Change Science
Fuel, Combustion & Flame
Fuel Processing Technology

All journals are available online via ScienceDirect: www.sciencedirect.com

To Contact the Publisher
Elsevier welcomes enquiries concerning publishing proposals: books, journal special issues, conference proceedings, etc. All formats and media can be considered. Should you have a publishing proposal you wish to discuss, please contact, without obligation, the publisher responsible for Elsevier's Energy program:

Henri van Dorssen
Publisher
Elsevier Ltd
The Boulevard, Langford Lane
Kidlington, Oxford
OX5 1GB, UK

Phone: +44 1865 84 3682
Fax: +44 1865 84 3931
E.mail: h.dorssen@elsevier.com

General enquiries, including placing orders, should be directed to Elsevier's Regional Sales Offices – please access the Elsevier homepage for full contact details (homepage details at the top of this page).

Carbon Dioxide Capture for Storage in Deep Geologic Formations – Results from the CO_2 Capture Project

Geologic Storage of Carbon Dioxide with Monitoring and Verification

Edited by

Sally M. Benson
Lawrence Berkeley Laboratory
Berkeley, CA,USA

and Associate Editors

Curt Oldenburg[1], Mike Hoversten[1] and Scott Imbus[2]
[1]Lawrence Berkeley National Laboratory
Berkeley, CA, USA
[2]Chevron Texaco Energy Technology Company
Bellaive, TX, USA

Volume 2

ELSEVIER
2005

Amsterdam – Boston – Heidelberg – London – New York – Oxford
Paris – San Diego – San Francisco – Singapore – Sydney – Tokyo

ELSEVIER B.V.
Radarweg 29
P.O. Box 211, 1000 AE Amsterdam
The Netherlands

ELSEVIER Inc.
525 B Street, Suite 1900
San Diego, CA 92101-4495
USA

ELSEVIER Ltd
The Boulevard, Langford Lane
Kidlington, Oxford OX5 1GB
UK

ELSEVIER Ltd
84 Theobalds Road
London WC1X 8RR
UK

First edition 2005

Library of Congress Cataloging in Publication Data
A catalog record is available from the Library of Congress.

British Library Cataloguing in Publication Data
A catalogue record is available from the British Library.

ISBN: 0-08-044570-5 (2 volume set)

Volume 1: Chapters 8, 9, 13, 14, 16, 17, 18, 24 and 32 were written with support of the U.S. Department of Energy under Contract No. DE-FC26-01NT41145. The Government reserves for itself and others acting on its behalf a royalty-free, non-exclusive, irrevocable, worldwide license for Governmental purposes to publish, distribute, translate, duplicate, exhibit and perform these copyrighted papers. EU co-funded work appears in chapters 19, 20, 21, 22, 23, 33, 34, 35, 36 and 37. Norwegian Research Council (Klimatek) co-funded work appears in chapters 1, 5, 7, 10, 12, 15 and 32.

Volume 2: The Storage Preface, Storage Integrity Preface, Monitoring and Verification Preface, Risk Assessment Preface and Chapters 1, 4, 6, 8, 13, 17, 18, 19, 20, 21, 22, 23, 24, 25, 26, 27, 28, 29, 30, 31, 32, 33 were written with support of the U.S. Department of Energy under Contract No. DE-FC26-01NT41145. The Government reserves for itself and others acting on its behalf a royalty-free, non-exclusive, irrevocable, worldwide license for Governmental purposes to publish, distribute, translate, duplicate, exhibit and perform these copyrighted papers. Norwegian Research Council (Klimatek) co-funded work appears in chapters 9, 15 and 16.

♾ The paper used in this publication meets the requirements of ANSI/NISO Z39.48-1992 (Permanence of Paper).
Printed in The Netherlands.

Carbon Dioxide Capture for Storage in Deep Geologic Formations, Volume 2
D.C. Thomas and S.M. Benson (Eds.)

Chapter 6

PREDICTING AND MONITORING GEOMECHANICAL EFFECTS OF CO_2 INJECTION

Jürgen E. Streit[1], Anthony F. Siggins[2] and Brian J. Evans[3]

[1]CRC for Greenhouse Gas Technologies, Australian School of Petroleum, The University of Adelaide, Adelaide, Australia
[2]CRC for Greenhouse Gas Technologies, CSIRO Petroleum, Perth, Australia
[3]CRC for Greenhouse Gas Technologies, Curtin University of Technology, Perth, Australia

ABSTRACT

Predicting and monitoring the geomechanical effects of underground CO_2 injection on stresses and seal integrity of the storage formation are crucial aspects of geological CO_2 storage. An increase in formation fluid pressure in a storage formation due to CO_2 injection decreases the effective stress in the rock. Low effective stresses can lead to fault reactivation or rock failure which could possibly be associated with seal breaching and unwanted CO_2 migration. To avoid seal breaching, the geomechanical stability of faults, reservoir rock, and top seal in potential CO_2 storage sites needs to be assessed. This requires the determination of in situ stresses, fault geometries, and frictional strengths of reservoir and seal rock. Fault stability and maximum sustainable pore fluid pressures can be estimated using methods such as failure plots, the FAST technique, or TrapTester (Badley Geoscience Ltd) software. In pressure-depleted reservoirs, in situ stresses and seal integrity need to be determined after depletion to estimate maximum sustainable pore fluid pressures. The detection of micro-seismic events arising from injection-induced shear failure of faults, fractures and intact rock is possible with geophone and accelerometer installations and can be used for real-time adjustment of injection pressures. In the event of injected CO_2 opening and infiltrating extensive fracture networks, this can possibly be detected using multi-component seismic methods and shear-wave splitting analysis.

INTRODUCTION

Underground storage of large quantities of anthropogenic CO_2 in geological formations is considered a viable option to significantly reduce greenhouse gas emissions [1,2]. One of the key objectives of geological CO_2 storage is the long-term underground containment of CO_2 in porous rock. To maximise storage quantities per unit volume of porous rock, CO_2 should be stored as a relatively dense phase in its supercritical state at depths below about 800 m [3]. Successful injection of CO_2 into a porous formation requires displacement or compression of the existing formation fluid and, thus, injection of CO_2 at pressures that exceed the formation pressure [4]. The excess pressure needs to be limited so it will not compromise the integrity of the reservoir seals.

It has been acknowledged by several authors that underground injection of CO_2 into porous rock at pressures higher than formation pressures can potentially induce fracturing and fault slip [5–7]. Indeed, it has been demonstrated that fluid injection into rocks can induce micro-seismic activity, as, e.g. in test sites such as the drill holes of the German continental deep drilling program (KTB) [8] or the Cold Lake oil field, Alberta [9]. Induced micro-seismicity is typically detected in the vicinity of the injector well within several hours to several days after fluid injection [8]. Deep well injection of waste fluids may even have induced earthquakes with moderate local magnitudes (M_L), as suggested for the 1967 Denver earthquakes ($M_L \leq 5.3$) [10] and

Abbreviations: FAST, fault analysis seal technology; MS, events, micro-seismic events; VSP, vertical seismic profiling.

the 1986/1987 Ohio earthquakes ($M_L \leq 4.9$) [11]. Seismicity that follows fluid injection is usually considered to result from increased pore fluid pressure in the hypocentral region of the seismic event [9,10].

Brittle failure of rocks and faults and associated micro-seismicity induced by overpressurisation would create or enhance fracture permeability while the formation of connected fracture networks and rough fault surfaces could provide pathways for unwanted CO_2 migration [12]. Thus, to avoid damage to top seal and fault seals due to injection-related pore pressure increase, maximum sustainable pore pressures need to be estimated for CO_2 injection. In addition, fluid pressures during injection as well as the CO_2 flow path should be monitored.

This chapter outlines key points of the geomechanical workflow that lead to assessments of fault stability and estimates of maximum sustainable fluid pressures in CO_2 storage sites. Monitoring of micro-seismic events, as well as seismic techniques suitable for the detection of unwanted CO_2 flow, are discussed as important methods for monitoring and controlling geomechanical effects of CO_2 injection.

STUDY METHODOLOGY

Some methods applicable to predict and monitor geomechanical effects of CO_2 injection were developed in the past to assist hydrocarbon exploration and production, while others are known from earthquake research and mining operations. Their application to CO_2 storage is new. The further development of such methods from different disciplines and their integration into a coherent and logical workflow is a key to facilitating sustainable storage of CO_2 in geological formations.

Predicting Geomechanical Effects of CO_2 Injection

The effect of increasing pore fluid pressure to decrease the strength of faults and rocks by decreasing effective stresses is extensively described in the geomechanical literature [13–15]. Geomechanical methods that are useful for estimating the stability of faults and maximum sustainable pore fluid pressures during CO_2 injection and storage are described below.

Effects of pore fluid pressure change on fault and rock stability

At depths greater than several hundred meters in the earth's crust, the maximum principal stresses usually are compressive. Where rocks contain pore fluid, the pressure of the pore fluid (P_f) acts in all directions and, thus, opposite to the compressive total stresses *(σ)* acting on the rock framework (Figure 1). Hence the pore fluid pressure combines with total stress to create a lower effective stress [13]:

$$\sigma' = \sigma - P_f \tag{1}$$

The effect of increasing pore fluid pressure on the state of stress on faults is schematically shown in Figure 2. When effective normal stresses ($\sigma_n - P_f$) are positive, they press opposing fault blocks together and resist sliding motion along the fault surface. Sliding can be induced by shear stresses (τ) acting parallel to the fault (Figure 2a). An increasing fluid pressure that decreases the effective normal stress therefore decreases the resistance to sliding. In a Mohr diagram, increasing pore fluid pressure shifts the Mohr circle towards the fault-failure envelope (Figure 2b). A relatively strong intact rock has a failure envelope further to the left from that of a relatively weak fault. Thus increasing fluid pressures often lead to fault failure before failure of relatively strong intact rock occurs. A failure envelope for a fault may be written in a general from as [14,18]

$$\tau_r = C + \mu(\sigma_n - P_f) \tag{2}$$

where τ_r is the shear stress that causes sliding and μ the coefficient of friction. C denotes an inherent shear strength of the fault which on cohesionless, gouge-lined fault surfaces is negligibly small [19]. On such faults, sliding occurs when the ratio of the shear stress to effective normal stress equals the coefficient of static friction of the fault:

$$\frac{\tau_r}{\sigma_n - P_f} = \mu \tag{3}$$

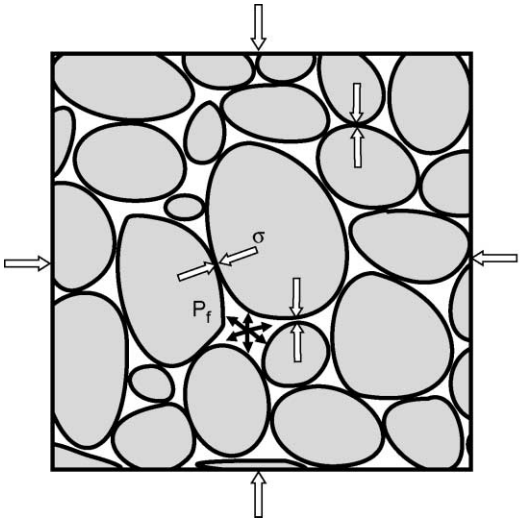

Figure 1: Sketch illustrating transmission of total stresses (σ) through grain boundaries and pore fluid pressure (P_f) acting in all directions, thus opposing total stresses. Diagram after Eisbacher [16].

The shear and effective normal stresses that act on a fault segment are a function of the fault geometry and are given in a two-dimensional form as

$$\tau = 0.5(\sigma_1 - \sigma_3)\sin\ 2\theta \text{ and } \sigma'_n = 0.5(\sigma'_1 + \sigma'_3) - 0.5(\sigma_1 - \sigma_3)\cos\ 2\theta \qquad (4)$$

where σ_1 and σ_3 are the maximum and minimum principal stresses, respectively, and θ the angle between the fault and σ_1 (Figure 2a). Since the shear and normal stresses that act on a fault depend on the fault angle θ, some faults are more favourably oriented for slip than others within a homogeneous stress field. The analysis of fault stability thus requires knowledge of the in situ stress tensor and the geometry of pre-existing faults.

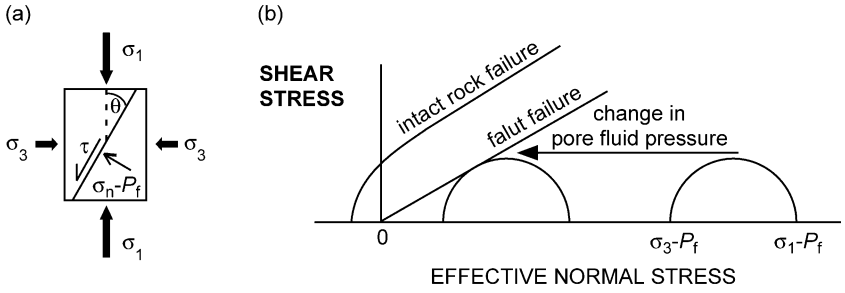

Figure 2: (a) Sketch showing the orientation of principal stresses, shear stress, and effective normal stress relative to a fault plane. (b) Mohr diagram showing shift of Mohr circle due to pore fluid pressure increase. Diagram from Streit and Hillis [17].

In situ stress determination
The orientation and magnitude of the vertical stress (S_v) and of the maximum (S_{Hmax}) and minimum horizontal stresses (S_{hmin}) can be determined from drilling data. It may be assumed that these stresses are principal stresses.

Stress orientation. The orientation of borehole breakouts (Figure 3a) which can be apparent on image logs and four-arm caliper logs can be used to derive the orientation of S_{Hmax} [21,22]. In cases where drilling-induced tensile fractures have formed, their orientation, which can be identified from image-log interpretation, directly indicates the orientation of S_{Hmax} (Figure 3b). The minimum horizontal stress and S_v are perpendicular to S_{Hmax}.

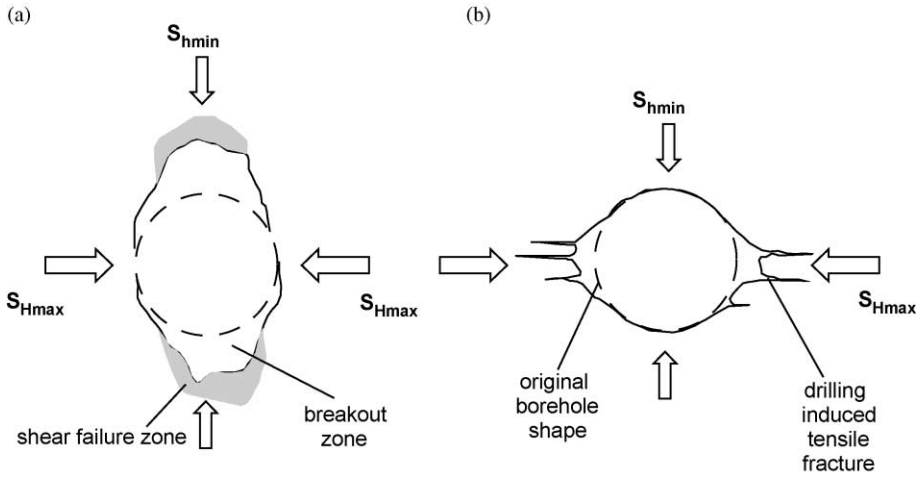

Figure 3: Schematic cross-section through borehole showing original circular borehole shape (broken line). (a) Borehole breakout due to spalling of borehole wall indicating the S_{hmin} direction. (b) Drilling-induced tensile fractures indicating the S_{Hmax} direction. Diagram modified from Dart and Zoback [20].

Stress magnitude. The overburden pressure at depth can be estimated by integrating the density of all overlying rocks and fluids over depth and calculating the resulting pressure [23]:

$$S_v = \int_z^0 \rho(z) g \; dz \tag{5}$$

S_v is the overburden pressure, g the gravitational acceleration (9.81 m/s^2), and z depth. ρ is the density of rocks and fluids. Rock densities can be obtained from density logs and check shot information on average sonic velocity. The overburden pressure is usually quoted as the average overburden (or vertical) stress gradient between the surface and the depth of interest. An example for a vertical stress profile is given in Figure 4.

The magnitude of S_{hmin} in wells can be estimated from fluid pressure levels attained during hydraulic fracturing of the formation [24]. Thus, S_{hmin} can be determined from hydraulic fracture tests and less ideally from leak-off tests, which are more commonly conducted.

The magnitude of S_{Hmax} can be constrained from the occurrence of borehole breakouts and drilling-induced tensile fractures, both of which can be interpreted on image logs [22,25]. Knowledge of the rock strength and the formation fluid pressure, as well as of the mud-weight during drilling and logging, is also required. However, estimates of S_{Hmax} are usually associated with relatively large uncertainty or cannot be obtained because the rock strength is not known.

In cases where S_{Hmax} cannot be determined, the stress regime may be constrained by applying a frictional limit calculation. This gives a crude upper bound on the magnitude of σ_1 based on the assumption that the strength of some optimally oriented faults within the area limits the magnitude of stresses that can accumulate. The limiting stress ratio for frictional sliding on optimally oriented faults can be written as [14]

$$\frac{\sigma_1 - P_\mathrm{f}}{\sigma_3 - P_\mathrm{f}} = ((\mu^2 + 1)^{1/2} + \mu)^2 \tag{6}$$

where P_f is the pore fluid pressure and μ the coefficient of static friction. An example for estimated frictional limits is given in Figure 4.

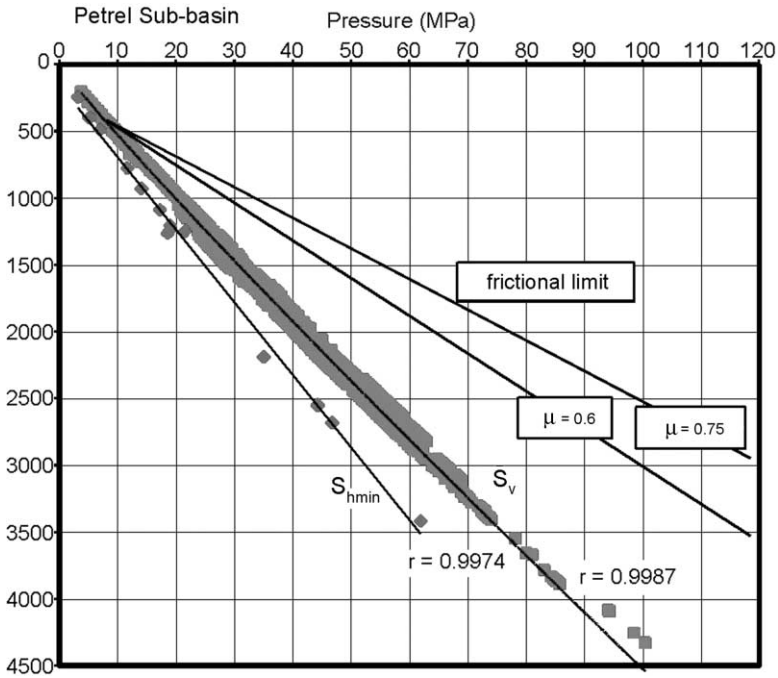

Figure 4: Stress profile for the Petrel Sub-basin based on drilling data. Estimates for S_{hmin} are based on pressures from leak-off tests; estimates for S_v were obtained by integrating density log data. Pearson correlation coefficients are indicated for curve fits. Frictional limits are indicated for different μ values. Diagram from Gibson-Poole et al. [6].

Fault stability and maximum sustainable pore fluid pressures in CO_2 storage sites

Assessments of fault stability require knowledge of fault geometries. Information on fault geometries in potential CO_2 storage sites is usually obtained from the structural interpretation of seismic data which need to be time-to-depth converted. Additional information on fracture geometry can be obtained from imaging fractures and faults that intersect wellbore walls. Such features may be imaged using, e.g. acoustic or ultrasonic scanners (borehole televiewers) or high-resolution resistivity imaging tools (FMS, FMI) in the wellbore.

Failure plots. Rock deformation experiments and field studies show that in some cases the formation of new fractures is more favourable than the reactivation of the pre-existing faults that have particular orientations

[26,27]. The orientation of relatively stable faults partly depends on the strength of their adjacent wall rock [14,28]. The orientation of relatively stable faults can be identified from failure plots [29,12], strictly for faults that contain the intermediate principal stress (σ_2) axis. It is further required that both fault and wall rock are subjected to the same stress and pore fluid pressure. This condition may hold for CO_2 storage scenarios.

The construction of failure plots for the identification of faults that are relatively stable is described in detail by Streit [29] for various rock types and fault strengths. Figure 5 shows failure plots for a hypothetical example in which faults are assumed to cut through Berea sandstone of the strength given by Handin et al. [13]. Figure 5 indicates that at a differential stress of 20 MPa, which is prevailing at approximately 2 km depth in some basins [30,31], faults with fault angles $>65°–75°$ are relatively stable. The failure plot method has been applied in two study sites of the Australian GEODISC program for CO_2 storage [6,32]. However, the tendency for fault slip to occur should also be estimated using 3D methods, especially for faults that cannot be identified as relatively stable.

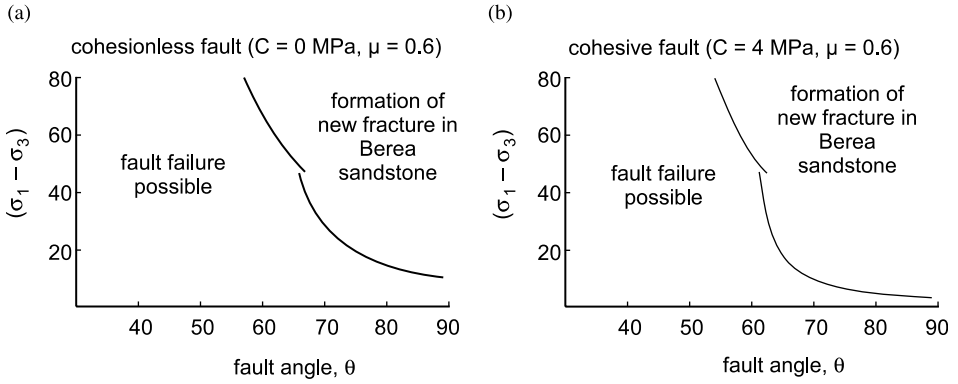

Figure 5: Failure plots showing differential stresses and fault angles that permit fault reactivation in the range $30 \leq \theta < 90$. Relatively stable faults fall in the fields that indicate the formation of new fractures. Figure from Streit and Hillis [12].

3D fault slip tendency. One way of assessing the potential for fault reactivation due to CO_2 injection is to determine the slip tendency of faults in the target area for CO_2 storage. By including the effect of pore fluid pressure, the slip tendency (T_s), which is defined as the ratio of resolved shear stress to normal stress acting on faults [33], may be expressed as:

$$T_s = \frac{\tau}{\sigma_n - P_f} \tag{7}$$

The slip tendency of a fault is evaluated by comparing the ambient stress ratio T_s to the stress ratio that would cause slip on a fault with no inherent shear strength ($C = 0$). Such a cohesionless fault is critically stressed when T_s equals the coefficient of static friction as shown in Eq. (3). Cohesionless faults are usually assumed to have Byerlee friction coefficients of $\mu = 0.6–0.85$ [22,34]. Where faults contain clay minerals, the friction coefficient can be less than $\mu = 0.6$ [18,35].

In cases where a 3D fault geometry can be constructed from the interpretation of depth-converted 3D seismic surveys or densely spaced 2D surveys, fault slip tendency can be calculated from Eq. (7) for each grid point on a fault. Figure 6 shows an example for the fault slip tendency computed from in situ stresses using commercially available software (TrapTester, Badley Geoscience Ltd, UK, http://www.badleys.co.uk).

Assuming that the two faults shown in Figure 6 have a coefficient of static friction of $\mu = 0.6$, their slip tendency is low to moderate. The maximum sustainable pore fluid pressure on these faults can be estimated by using progressively higher pore fluid pressures in Eq. (7) until the slip tendency becomes critically high.

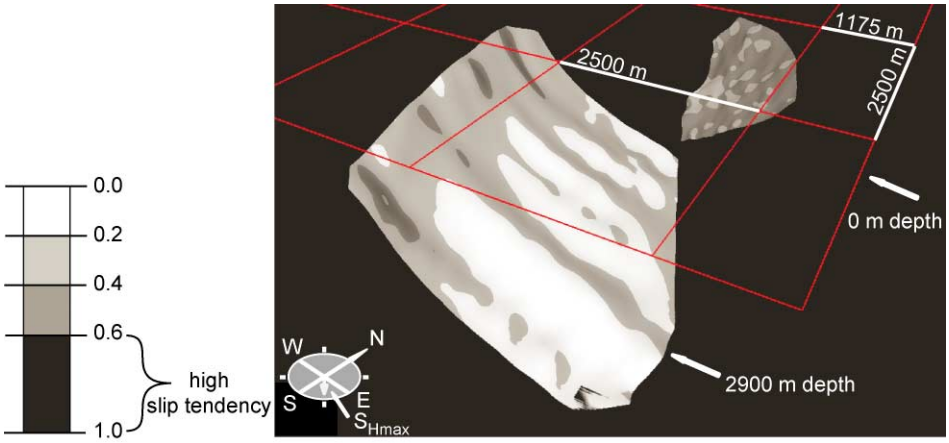

Figure 6: Slip tendency on two fault surfaces for $S_{\text{hmin}} = 15.2z + 0.5$, $S_{\text{v}} = S_{\text{Hmax}} = 22.5z + 0.5$, and $P_{\text{f}} = 9.7z + 0.5$ (z = depth in km); S_{Hmax} orientation is 116°N.

Critical pore fluid pressure increase. The likelihood for fault failure can be estimated by calculating the fluid pressure increase required to induce brittle failure (ΔP_{f}). This fluid pressure increase can be shown in a 3D Mohr diagram [14] for any fault angle (θ) as illustrated in Figure 7.

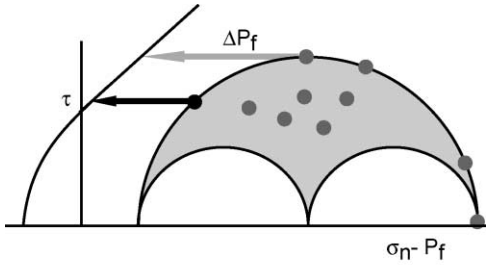

Figure 7: Illustration of state of stress on faults with different geometries in a 3D Mohr diagram and required pore pressure changes (ΔP_{f}) to reactive such faults. Diagram modified from Mildren et al. [31].

The FAST (Fault Analysis Seal Technology) technique of Mildren et al. [31] is used herein to illustrate the fluid pressure increase required for fault failure to occur (ΔP_{f}). This fluid pressure increase is calculated for a particular depth and shown in a southern hemisphere polar plot projection. The orientation of poles to fault planes in such a projection can then be attributed to the relevant ΔP_{f} value (Figure 8). Since the FAST technique can include an inherent shear strength of a fault or rock (C), it can also be used to estimate fluid pressures that induce failure in intact reservoir rock or seal [31]. The technique is thus suitable to calculate maximum sustainable pore fluid pressures on faults, in intact reservoir rock, and below top seals, given that

the relevant rock or fault frictional strength is known. Application of the FAST technique on a study site for potential CO_2 storage is given by Gibson-Poole et al. [32].

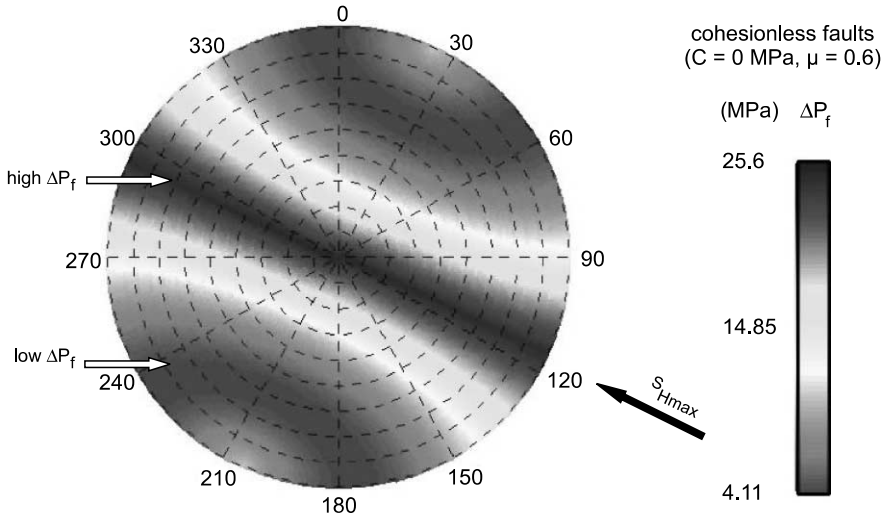

Figure 8: Polar plot projection showing pore fluid pressure increases required to cause failure for any fault orientation (poles to planes) at 2 km depth using the same stress tensor as in Figure 6. Faults are assumed to be cohesionless with $\mu = 0.6$.

Monitoring for Induced Shear Failure

Geophysics of micro-seismic events

In cases where fluid injection induces shear fracturing or fault slip at a seismic rate, micro-earthquakes can occur [36,37]. These micro-earthquakes are commonly termed "micro-seismic" (MS) events and can be readily monitored with geophysical instrumentation such as accelerometer, hydrophone or geophone arrays. Such instrumentation provides a means of visualising the location in 3D, the time, and the magnitude of the events. As has been well established in 15 years of monitoring of hydraulic fracturing experiments in Hot Dry Rock fields, the cloud of MS events can be associated with fractures associated with advancing fluid fronts [38]. Similar responses have been observed in hydrocarbon fields during production and water flooding. This then has provided a new means of reservoir characterisation termed seismicity-based reservoir characterisation.

Micro-seismic events arise when a sudden inelastic deformation occurs such as slip on a fracture or fault (Figure 2a). During slip the elastic strain energy stored in the rock is transformed into fracture surface energy, heat energy, and the radiation of seismic waves. The rate at which this transformation occurs determines the frequency of emission and efficiency of the radiating process. The micro-seismic event will be accompanied by stress release in the zone of the rupture [39].

Slip on a pre-existing fracture in a rock mass will generate a radiating seismic wavefield consisting of both compressional, P, and shear, S, wavelets. The bulk of the seismic energy generated will consist of S-waves (this will be manifested in the high S to P-wave amplitude ratio). Waveforms recorded will contain a superposition of primary P and S wavelets followed by secondary P and S components arising from reflections and refractions within the reservoir formations. Figure 9 illustrates the P-wave and S-wave radiation patterns from a double couple acting within an isotropic rock mass.

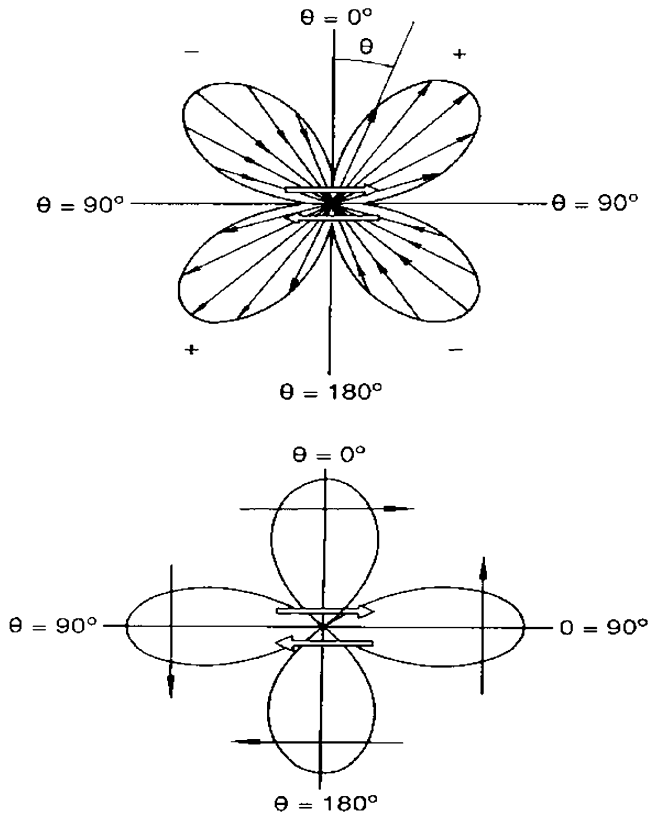

Figure 9: (a) Radiation pattern of the P-wave displacement at the source of a micro-seismic event. The P-wave lobes are shown in a plane of constant azimuth. The force couples are represented by central arrows. (b) Radiation pattern of the S-wave displacement at the source of a micro-seismic event shown in a plane of constant azimuth. The central arrows represent the force couple, giving rise to the event while the larger arrows represent the direction of particle displacement. After Aki and Richards [40].

Monitoring micro-seismic events

Most transducers used for monitoring micro-seismic activity are based on triaxial geophones, usually installed downhole. It is desirable to have at least six triaxial seismometers installed in a monitoring well in close proximity to the injection well. For long-term monitoring, some near-surface arrays are desirable although the geology of the field will influence the design of the arrays.

In recent times the "instrumented oil field" has moved from a concept to reality. It is rapidly gathering impetus with the development of a new generation of transducers. The aim of the instrumented field is to monitor changes in temperature, pressure, and seismic response over the life of a reservoir with arrays of permanently installed transducers. A recent trend has been to develop fibre-optics-based instrumentation that avoids the fragility of down-hole electrical connections over long periods. While temperature and pressure-measuring fibre-optics-based devices are relatively well established, a new type of seismometer that relies on optical diffraction has been developed and installed recently (Internet News Release—Weatherford.com). In the light of such technological advances, fibre-optics-based permanent installations

for monitoring micro-seismic activity as well as the usual reservoir parameters, such as temperature and pressure, are strongly recommended for all subsurface CO_2 storage reservoirs.

Interpretation of transducer recordings
With sufficient number and distribution of receiver stations arranged in space around the source, it is theoretically possible to determine the radiation pattern, i.e. the P-wave and S-wave radiation pattern lobes, associated with a particular event and its orientation. This is usually represented graphically by equal area hemispherical projections. This allows the elements of the moment tensor to be calculated and consequently the fault plane orientation, as is illustrated in Figure 9. The procedure to determine the slip magnitude and orientation from an event is termed a "moment tensor inversion" and is described in depth in Ref. [41].

In the case of a small number of receivers, such as the arrays used in monitoring hydraulic fracturing, it is not possible to determine the full moment tensor. Instead, fault plane solutions derived from the first-motion polarities of P-waves and also S-waves can be determined by graphical means. This procedure consists of plotting the ray path vectors to each receiver station as points of compressional (P) or dilatational polarity (T) on to a hemispherical projection. It then becomes a matter of determining the best fit to the two orthogonal planes that separate the compressional and dilatational points. These two planes are termed

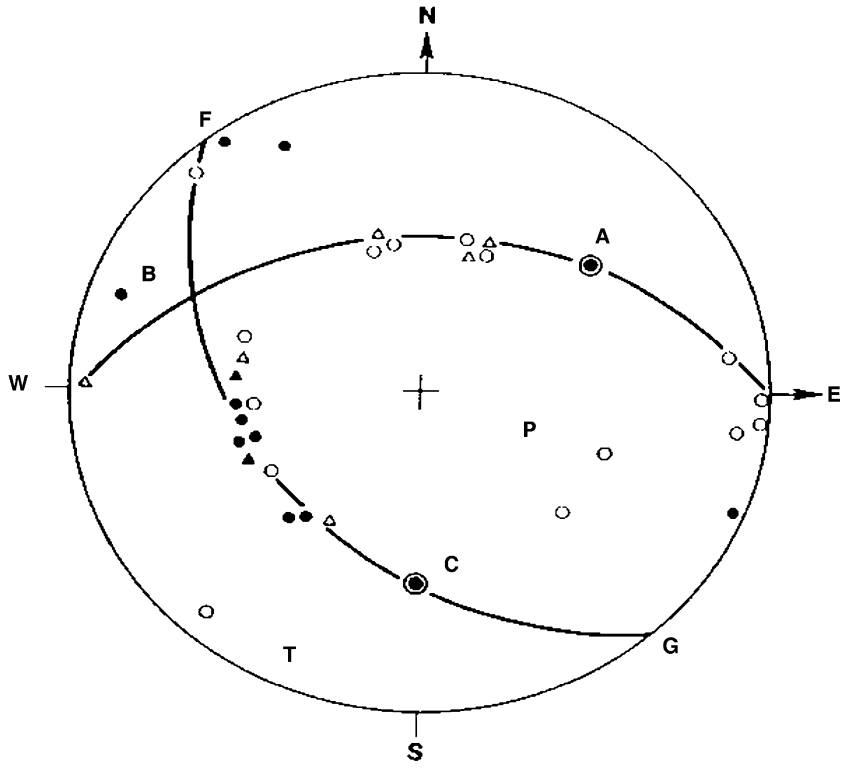

Figure 10: Fault plane solution from Gibowicz and Kijko [39] for a mining-related seismic event. A lower hemisphere equal area projection is used. Solid circles and triangles represent compressional arrivals while open circles and triangles represent dilatational arrivals. A and C are the poles of the two nodal planes. P and T are the axes of compression and tension, respectively.

the focal plane solution and comprise the fault plane and an equivalent orthogonal or auxiliary plane. Additional information such as structural geological information is needed to resolve the ambiguity. A typical fault-plane solution is presented in Figure 10.

Attempts to find fault-plane solutions are rarely reported in the literature that is related to micro-seismic monitoring during hydraulic fracturing. Instead the emphasis is placed on source location producing the conventional MS cloud. This is not surprising given the difficulty in achieving a spatial distribution of receivers that would give a fault-plane solution. However, if fault-plane solutions can be achieved, valuable information can be obtained concerning the orientation of the fault planes and the slip or shearing along those planes. A number of new analysis techniques have been developed which have allowed for very high spatial resolution of MS events. These techniques have greatly improved the visualisation of the intricate detail of subsurface fluid-flow associated with seismic slip [42–44]. Hence, the monitoring for MS events in CO_2 storage sites will be useful for detecting injection-induced slip on faults and fractures and for real-time adjustment of injection pressures.

Seismic Methods for Detecting CO_2 Migration into Fractures

Seismic methods

Surface seismic methods are the most dominant methods used to image underlying geological features, predict lithological variations, and detect the presence of hydrocarbons. Presently most of the surveys are 3D. Successful application of three-component (3C) surveys on land has led to similar, but far more complex, data acquisition procedures offshore. These are designed to record both pressure and particle velocities by utilising hydrophones and 3C geophones and are called 4C and are often 3D. Repeated surveys (usually 3D, 1C or 4C) are useful for monitoring hydrocarbon production and reservoir stimulation by detecting changes in fluid type, saturation, and pressure.

Seismic methods can also be applied in boreholes as, e.g. the vertical seismic profiling (VSP) method. The information obtained by this method is limited to a relatively small area around the borehole in comparison to an area typically covered by surface seismic methods. However, a VSP survey, unlike surface seismic surveys, is useful for recording transmitted waves, from which one can deduce rock properties.

Detection of fracture systems

In practice, a wide area around a borehole can be analysed through multi-azimuth, multi-offset 3C VSP measurements. However, over large areas, the detection of aligned fractures, their density and fill requires repeated 3D (time lapse 3D or "4D") surface seismic data, using single or multi-component recording and analysis methods.

One option for fracture detection and characterisation is the use of P-wave surveys. Many authors [45,46,47] have theoretically studied the behaviour of P-waves (amplitude, velocity, and frequency) propagating through fractured media, the results of which have been corroborated by researchers such as Nur and Simmons [48] and Sayers and Ebrom [49]. P-waves propagating parallel to fractures are subject to rock stiffness but across the fractures they encounter rock compliance (weakness). This results in azimuthally dependent P-wave velocities, amplitudes, and attenuation.

3D surface seismic data are suitable for the detection of P- and S-wave azimuthal anisotropies such as caused by fractures. A polar representation of 3D azimuthal normal move-out velocity will result in an ellipse, with semi-major axis being collinear with the fracture direction [50]. The elongation of the ellipse depends on fracture parameters such as fracture density, fracture aspect ratio, and fluid content. Figure 11 shows Thomsen's anisotropy parameters computed for dry and saturated fractures using different fracture densities. Thomsen's anisotropy parameters [46] are given by

$$\gamma \equiv \frac{c_{66} - c_{55}}{2c_{55}};\ \varepsilon \equiv \frac{c_{11} - c_{33}}{2c_{33}};\ \delta \equiv \frac{(c_{13} + c_{55})^2 - (c_{33} - c_{55})^2}{2c_{33}(c_{33} - c_{55})} \tag{8}$$

where c_{ij} are elastic stiffness values, ε and γ describe P- and S-wave anisotropies, respectively, through the differences between vertical and horizontal velocities. Parameter δ is considered to control the shape of

the P-wave group-velocity surface away from normal incidence [47]. Simple models as presented in Figure 11 show that the difference in P-wave anisotropy (ε) between dry and fluid saturated fractures is considerable for high fracture densities. Azimuthal variations in P-wave amplitudes are also a tool for the detection and characterisation of fractures [51,52].

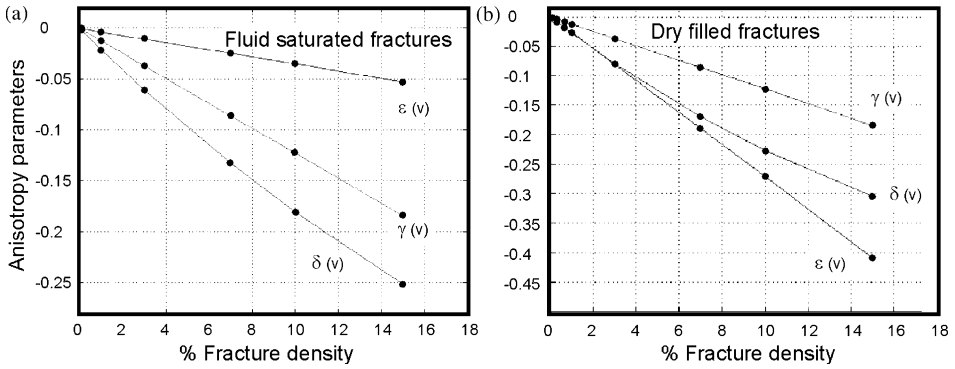

Figure 11: Variations of Thomsen anisotropy parameters $\varepsilon^{(V)}$, $\delta^{(V)}$ and $\gamma^{(V)}$ for horizontal transverse isotropic media with fracture density for a fixed aspect ratio: (a) fluid saturated fractures and (b) dry fractures. Note a high value of the fractional P-wave anisotropy $\varepsilon^{(V)}$ for a system of dry fractures of high density and $\varepsilon^{(V)} - \delta^{(V)} \cong 0$, which is the case of elliptical anisotropy. Also $\varepsilon^{(V)} - \gamma^{(V)}$ is positive for fluid saturated and negative for dry fractures.

Detection of CO_2-filled fractures and faults

P-waves can be utilised for the detection of fractures, their alignment, their properties, and their fluid contents through measurements of velocity, amplitude, attributes, and attenuation in different directions and incidence angles [50,53,54]. In practice, conventional 3D P-wave (particularly marine) surveys lack the range of azimuths and incidence angles required for comprehensive studies of fracture properties. In addition, a successful application of the P-wave methodology is strongly affected by seismic signal-to-noise ratio, and time-lapse P-wave imaging may not be effective at depths where CO_2 properties are similar to liquids. In such cases, the application of borehole time-lapse surveys using VSP and cross-well methods is useful. The frequency content of cross-well seismic and vertical sampling provides data having a vertical resolution comparable to that of wire-line logging. A disadvantage of the cross-well method is that only the 2D slice between the wells can be imaged and the areal extent of a VSP is also therefore limited.

Cross-well pre-stack depth migration using all body waves is useful for detecting small-scale faults and for detailed lithological interpretation. This method can be applied to detect CO_2 migration into vertical faults and fractures. Permanent seismic array deployment allows time-lapse cross-well seismic P- and S-wave recording methods to image-isolated fractures and faults during CO_2 flooding as shown by Wang et al. [55]. This technique works well in high-velocity, high-Q carbonates, but not in all formations.

A method that can be applied to detect aligned fractures is shear wave polarisation analysis (from 3C VSP surveys). This method provides clues on fracture alignment through variations in elastic properties, but this is non-unique due to the alignment of pore space by the in situ stress field. In aligned fracture systems, the shear wave splits into two modes—"fast S1" and "slow S2"—which are polarised along and perpendicular to fractures as suggested by Crampin [56]. The difference in travel time between these two modes is proportional to open fracture density.

Shear wave splitting away from symmetry directions that are parallel or perpendicular to the fracture planes is dependent on the nature of the fluid saturation [45,57]. Shear wave energy would be unaffected by the CO_2 state of phase, but shear wave polarisation, their velocities, and frequency content may change with

saturation. Hence time-lapse multi-component VSP surveys using permanently installed 3C geophones may be most useful for the detection of CO_2 infiltration into fractures.

Field Examples

Multi-component seismic data recorded at the Vacuum Field, New Mexico, have shown changes in S-wave splitting within fractured carbonates in response to changes in pore pressure [58]. The interpretation of the results was that the opening of the fractures due to pore pressure increase at the injection well produces an increase in S-wave anisotropy. At the production well a decrease in pore pressure has the opposite effect on the split shear waves. Similar observations were reported during the Lost Hills CO_2 flood where CO_2 was observed to preferentially flow along fracture networks [59]. These examples show that multi-component seismic and in particular shear-wave polarisation analysis have a great potential for detecting migration of CO_2 into highly fractured zones. However, such analyses are unlikely to detect thin CO_2 accumulations in single fractures and faults with typical millimetre to centimetre-scale apertures.

DISCUSSION

This article focuses on the geomechanical effects of CO_2 injection that arise from the law of effective stress (see Eq. (1)). Other stress changes that can result from fluid pressure changes and which are not described by Eq. (1) are briefly discussed in this section. In addition, some key uncertainties that can affect the prediction of fault stability and maximum sustainable fluid pressures will be addressed.

Uncertainty in Rock Frictional Strength

The frictional strength of faults at depth in potential CO_2 storage sites, such as depleted gas reservoirs or saline formations, is difficult to determine. Core samples from faults are rarely available and unlikely to be representative for all faults in the vicinity of a CO_2 storage site. Thus geomechanical predictions, which are usually based on empirical frictional values, need to allow for variations in frictional properties of faults. The frictional strength of reservoir rock and top seal can be determined in laboratory measurements. This requires either rock samples from outcrops of the relevant lithological units of interest, or, even better, fresh core samples from wells in the relevant CO_2 storage site.

Aseismic Slip

While transducer recordings can be used to monitor for seismic slip on fractures and faults, other methods are required to detect aseismic fault slip or so-called fault creep. Appropriate methods include the installation of tiltmeters downhole and creepmeters across fault surface traces, as well as the repeated GPS surveying of reference stations in order to detect fault movement. However, to determine whether any detectable fault creep is related to fluid injection, pre-injection long-term monitoring would be required. Since fault creep may not significantly increase fault permeability and is not the primary study objective, it appears more practical to conduct seismic monitoring for CO_2 migration into faults and near-surface testing (e.g. soil gas testing) for excessive CO_2 accumulations.

Pore Pressure/Stress Coupling

Pressure depletion associated with production in hydrocarbon fields can be associated with a decrease in the total minimum horizontal stress [60,61]. While the vertical stress is usually assumed to remain essentially unaffected during pore pressure depletion, a change of only the horizontal total stresses can, in some tectonic settings, affect the shear stress acting on faults and rocks [61]. This is indicated in Figure 12 for normal fault stress regimes. Induced stress changes are thought to be the cause of faulting within and in the vicinity of reservoirs subjected to pore pressure depletion [60,62].

The effects of pore pressure/stress coupling are of relevance to geological CO_2 storage for a number of reasons. In cases where CO_2 storage is envisaged in pressure-depleted reservoirs, failure that was induced due to pore pressure/stress coupling during reservoir depletion can have compromised the integrity of seals and thus affect the suitability of the reservoir for CO_2 storage.

In addition, the compaction of reservoir rock that can occur due to severe pressure depletion can be partly elastic and also partly permanent [63]. In cases of permanent compaction (= pore collapse) the potential storage capacity for CO_2 would be diminished. Since pore pressure depletion can affect the in situ horizontal

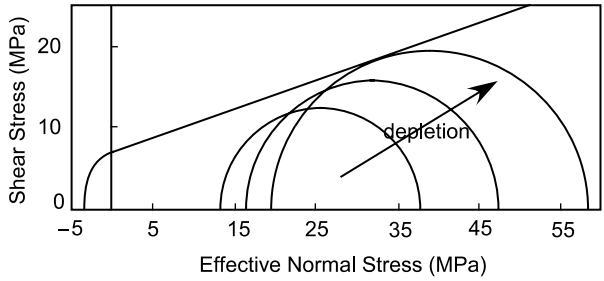

Figure 12: Mohr diagram showing the effect of pore pressure/stress coupling during pore pressure depletion in a normal fault stress regime. For the shown stress path, pressure depletion leads to failure due to decreases of S_{hmin}. Diagram from Hillis [61].

stresses, their orientation and magnitude need to be determined from post-production data in order to be useful for the evaluation of fault stability and maximum sustainable fluid pressures.

Pore pressure/stress coupling that is known to occur during pore pressure depletion may also occur during fluid injection. Since little is known about the poroelastic response of entire reservoirs to fluid pressure increase and the potential effects on total horizontal stresses this needs to be investigated during fluid injection in CO_2 storage sites [12,17].

CONCLUSIONS

This study has presented methods that can be used to predict and monitor geomechanical effects of underground CO_2 injection. The focus was the assessment of fault stability, the prediction and monitoring of maximum sustainable fluid pressures, and the application of seismic methods for the detection of CO_2 infiltration into fault-fracture networks.

The main conclusions of this study are:

- Low effective stresses can lead to fault reactivation at pore fluid pressures lower than those required to induce new fractures in intact rock, especially where faults are optimally oriented for reactivation.
- The effective stresses prevailing in potential CO_2 storage sites can be constrained from the interpretation of drilling data and the application of failure criteria for faults and wellbores.
- Utilising the information on the effective stresses in potential CO_2 storage sites and relevant rock strength data, the stability of faults and rocks and maximum sustainable fluid pressures can be estimated using techniques such as failure plots, FAST, and TrapTester software.
- For CO_2 storage in pressure-depleted reservoirs or fields, these need to be tested for depletion-related effects including damage to seals, permanent compaction of pore space, and stress changes.
- Reliable predictions of poroelastic responses of reservoir rocks to CO_2 injection-related pressure increases and any potentially related changes of total stresses need further studies.
- Seismometer monitoring of micro-seismic events in CO_2 storage sites is an ideal option for fast detection of induced faulting and fracturing related to CO_2 injection and associated effective stress changes.
- Active seismic monitoring methods (multi-component seismic methods and shear-wave splitting) are useful for detecting and monitoring CO_2 accumulations in porous reservoir rock and overburden, or in extensive fault-fracture networks, but may not be suitable for detecting the opening of isolated fractures and faults with millimetre to centimetre-scale widths.

RECOMMENDATIONS

Measures that should be taken for CO_2 storage include the assessment of fault and rock stabilities and the estimation of maximum sustainable fluid pressures in reservoir rock, on faults, and below top seals. Due to

the usually sparse availability of testable rock samples, geomechanical and physical predictions need to allow for variations in rock and fault properties. Seismic methods should be applied to detect induced brittle failure that causes micro-seismic events and to identify significant CO_2 accumulations in extensive fracture networks. Thus, the permanent installation of acoustic transducers that record micro-seismicity is recommended for monitoring in CO_2 storage sites. Since the thickness of layered CO_2 accumulations that can be detected by active seismic monitoring methods is limited, monitoring for leak detection requires a combination of seismic and non-seismic monitoring methods.

ACKNOWLEDGEMENTS

This work is based on research undertaken for the CO_2 Capture Project (CCP) under subcontract T-1.1.4 and also based on research conducted by the Australian CRC for Greenhouse Gas Technologies (CO2CRC). The authors appreciate helpful discussions with R.F. Daniel, D.N Dewhurst, K. Dodds, R.R. Hillis, and M. Urosevic. Badley Geoscience Ltd. kindly provided *TrapTester* software. Comments on the manuscript by Curt Oldenburg (Associate Editor) and two anonymous reviewers are appreciated.

REFERENCES

1. S. Bachu, *Energy Convers. Manage.* **41** (2000) 953.
2. P.J. Cook, A. Rigg, J. Bradshaw, *APPEA J.* **40** (2000) 654.
3. S. Holloway, *Energy Convers. Manage.* **37** (1996) 1149.
4. S. Holloway, R. van der Straaten, *Energy Convers. Manage.* **36** (1995) 519.
5. P.D. Bergman, E. Winter, *Energy Convers. Manage.* **36** (1995) 523.
6. C.M. Gibson-Poole, S.C. Lang, J.E. Streit, G.M. Kraishan, R.R. Hillis, in: M. Keep, S.J. Moss (Eds.), The Sedimentary Basins of Western Australia 3: *Proceedings of the Petroleum Exploration Society of Australia Symposium*, Perth, WA, 2002, 2002, p. 439.
7. J. Sminchak, N. Gupta, C. Byrer, P. Bergman, *J. Energy Environ. Res.* **2** (2002) 32.
8. S.A. Shapiro, E. Huenges, G. Borm, *Geophys. J. Int.* **131** (1997) F15.
9. S. Talebi, T.J. Boone, J.E. Eastwood, *Pure Appl. Geophys.* **153** (1998) 95.
10. J.H. Healy, W.W. Ruby, D.T. Griggs, C.B. Raleigh, *Science* **161** (1968) 1301.
11. M.U. Ahmad, J.A. Smith, *Geology* **16** (1988) 739.
12. J.E. Streit, R.R. Hillis, in: J. Gale, Y. Kaya (Eds.), *Proceedings of the Sixth International Conference on Greenhouse Gas Control Technologies*, *1–4 October 2002*, Kyoto, Japan, vol. I, Pergamon Press, Amsterdam, 2003, p. 495.
13. J. Handin, R.V. Hager Jr., M. Friedman, J.N. Feather, *Am. Assoc. Petrol. Geol. Bull.* **47** (1963) 718.
14. J. Jaeger, N.G.W. Cook, Fundamentals of Rock Mechanics, Chapman & Hall, London, 1979.
15. J.E. Streit, *J. Geophys. Res.* **102** (1997) 24619.
16. G.H. Eisbacher, Einführung in die Tektonik, Enke, Stuttgart, 1996.
17. J.E. Streit, R.R. Hillis, Energy, **29**(9–10) (2004), 1445–1456.
18. J. Byerlee, Friction of rocks, *Pure Appl. Geophys.* **116** (1978) 615.
19. T. Shimamoto, J.M. Logan, *J. Geophys. Res.* **86** (1981) 2902.
20. R.L. Dart, M.L. Zoback, *Log Analyst* **30** (1989) 12.
21. R.A. Plumb, S.H. Hickman, *J. Geophys. Res.* **90** (1985) 5513.
22. D. Moos, M.D. Zoback, *J. Geophys. Res.* **95** (1990) 9305.
23. A. McGarr, N.C. Gay, *Ann. Rev. Earth Planet. Sci.* **6** (1978) 405.
24. T. Engelder, Stress Regimes in the Lithosphere, Princeton University Press, Princeton, NJ, 1993.
25. P. Peska, M.D. Zoback, *J. Geophys. Res.* **100** (1995) 12791.
26. J. Handin, *J. Geophys. Res.* **74** (1969) 5343.
27. A. Nur, H. Ron, O. Scotti, *Geology* **14** (1986) 746.
28. R.H. Sibson, *J. Struct. Geol.* **7** (1985) 751.
29. J.E. Streit, *J. Geophys. Res.* **104** (1999) 17929.
30. A.D. Castillo, R.R. Hillis, K. Asquith, M. Fischer, in: P.G. Purcell, R.R. Purcell (Eds.), The Sedimentary Basins of Western Australia 2—Proceedings of Petroleum Exploration Society of Australia Symposium, Perth, WA, 1998, p. 325.
31. S.D. Mildren, R.R. Hillis, J. Kaldi, *APPEA J.* **42** (2002) 187.

32. C.M. Gibson-Poole, J.E. Streit, S.C. Lang, A.L. Hennig, C.J. Otto, *APPEA J.* **44** (2004) 653.
33. A. Morris, D.A. Ferrill, D.B. Henderson, *Geology* **24** (1996) 275.
34. R.H. Sibson, in: C.J. Marone, M.L. Blanpied (Eds.), Faulting, Friction, and Earthquake Mechanics, Part I Pageoph Topical Volumes, Birkhäuser Verlag, Basel, 1994, p. 645.
35. T. Shimamoto, J.M. Logan, *Tectonophysics* **75** (1981) 243.
36. S.A. Shapiro, *Geophys. J. Int.* **143** (2000) 931.
37. P. Talwani, S. Acree, *Pure Appl. Geophys.* **122** (1985) 947.
38. T. Wallroth, A. Jupe, R. Jones, *Marine Petrol. Geol.* **13** (4) (1996) 447.
39. S.J. Gibowicz, A. Kijko, An Introduction to Mining Seismology, Academic Press, New York, 1994.
40. K. Aki, P.G. Richards, Quantitative Seismology. Theory and Methods, Freeman, New York, 1980.
41. J.A. Snoke, in: W.H.K. Lee, H. Knanamori, P.C. Jennings, C. Kisslinger (Eds.), International Handbook of Earthquake Engineering Seismology, Academic Press, San Diego, 2003.
42. W.S. Phillips, L.S. House, M.C. Fehler, *J. Geophys. Res.* **102** (1997) 11745.
43. H. Moriya, H. Niitsuma, R. Baria, *Bull. Seism. Soc. Am.* **93** (1996) 1606.
44. R.A Jones, R.C. Stewart, *J. Geophys. Res.* **102** (1997) 8245.
45. J.A. Hudson, *Geophys. J. R. Astron. Soc.* **64** (1981) 133.
46. L. Thomsen, *Geophysics* **51** (1986) 1954.
47. L. Thomsen, *Geophysics* **53** (1988) 304.
48. A. Nur, G. Simmons, *J. Geophys. Res.* **74** (1969) 6667.
49. C.M. Sayers, D.A. Ebrom, *Geophysics* **62** (1997) 1570.
50. V. Grechka, I. Tsvankin, *Geophysics* **63** (1998) 1079.
51. W. Chen, AVO in azimuthally anisotropic media fracture detection using P-wave data and a seismic study of naturally fractured tight gas reservoirs, unpublished PhD thesis, Stanford University, 1995.
52. M. Luo, B.J. Evans, *64th Meeting: European Association of Geoscience Engineering*, 2002, p. C043.
53. C.M. Sayers, J.E. Rickett, *Geophys. Prosp. Eur. Assoc. Geosci. Eng.* **45** (1997) 165.
54. A. Bakulin, C. Slater, H. Bunain, V. Grechka, *70th Annual International Meeting, Society of Exploratory Geophysics*, 2000, p. 1405.
55. Z. Wang, M.E. Cates, R.T. Langan, *Geophysics* **63** (1998) 1604.
56. S. Crampin, *Wave Motion* **3** (1981) 343.
57. L. Thomsen, *Geophysics* **43** (1995) 805.
58. L. Duranti, T.L. Davis, R.D. Benson, *70th Annual International Meeting, Society of Exploratory Geophysics*, Expanded Abstracts, 2000, 1528.
59. P.R. Perri, DOE/BC/14938-12 (OSTI ID: 5127), *2001 Annual Report, National Petroleum Technology Office*, US Department of Energy, Tulsa, OK, 2002.
60. L.W. Teufel, D.W. Rhett, H.E. Farrell, in: J.-C. Roegiers (Ed.), Rock Mechanics as a Multidisciplinary Science: *Proceedings of the 32nd US Symposium*, Balkema, Rotterdam, 1991, p. 63.
61. R.R. Hillis, *Expl. Geophys.* **31** (2000) 448.
62. P. Segall, *Geology* **17** (1989) 942.
63. P. Johnson, D.W. Rhett, W.T. Siemers, *J. Petrol. Tech.* **July** (1989) 712.